


Weyl excitations via helicon-phonon mixing in conducting materials

Dmitry K. Efimkin^{1,2,*} and Sergey Syzranov³

¹*School of Physics and Astronomy, Monash University, Victoria 3800, Australia*

²*ARC Centre of Excellence in Future Low-Energy Electronics Technologies, Monash University, Victoria 3800, Australia*

³*Physics Department, University of California, Santa Cruz, California 95064, USA*

 (Received 20 December 2022; revised 6 October 2023; accepted 9 October 2023; published 30 October 2023)

Quasiparticles with Weyl dispersion can display an abundance of novel topological, thermodynamic, and transport phenomena, which is why novel Weyl materials and platforms for Weyl physics are being intensively looked for in electronic, magnetic, photonic, and acoustic systems. We demonstrate that conducting materials in magnetic fields generically host Weyl excitations due to the hybridization of phonons with helicons, collective neutral modes of electrons interacting with electromagnetic waves propagating in the material. Such Weyl excitations are, in general, created by the interactions of helicons with longitudinal acoustic phonons. An additional type of Weyl excitation in polar crystals comes from the interaction between helicons and longitudinal optical phonons. Such excitations can be detected in x-ray and Raman scattering experiments. The existence of the Weyl excitations involving optical phonons in the bulk of the materials also leads to the formation of topologically protected surface arc states that can be detected via surface plasmon resonance.

DOI: [10.1103/PhysRevB.108.L161411](https://doi.org/10.1103/PhysRevB.108.L161411)

Introduction. The tremendous recent interest in Weyl materials [1–10] is owed, in large part, to a plethora of fundamental and novel topological phenomena they can display: the chiral anomaly [11,12], topological surface states [1,2], unconventional regimes of transport [13–17], etc. Numerous predictions and observations of Weyl-related topological phenomena have motivated researchers to look for Weyl excitations not only in electronic but also in magnetic, photonic, and acoustic systems.

Excitations with Weyl dispersion may generically be engineered via the hybridization of two other types of excitations with similar energies if the interactions between them vanishes along a certain direction of momentum. Such interactions lead to a degeneracy between the two bands of the hybridized excitations at the respective wave vectors and a gap for other wave vectors. For example, the hybridization between different types of plasma waves [18,19] has been shown to lead to Weyl excitations in photonic metamaterials [20–22] and magnetized electron gases [23–26]. This mechanism of the formation of Weyl excitations is similar to the emergence of 2D topological excitations due to the hybridization between phonons and spin waves [27–34], spin and plasma waves [35], as well as excitons and cavity photons [36,37].

In this Letter, we demonstrate that conducting materials in magnetic fields generically host Weyl excitation due to the hybridization of phonons with helicons [18,19], collective neutral modes of electrons interacting with electromagnetic waves propagating in the material. Such Weyl excitations emerge generically due to the hybridization of helicons with longitudinal acoustic phonons. In polar crystals, Weyl exci-

tations are also created by the interactions of helicons with longitudinal optical phonons.

The predicted Weyl excitations can be detected in, e.g., Raman spectroscopy experiments. Weyl excitations involving optical phonons in the bulk of the material also lead to the formation of topologically protected arc states on its surfaces, which can be observed via the surface plasmon resonance.

Heuristic argument for the emergence of Weyl nodes. A conductor in a magnetic field hosts excitations called *helicons* [18] that exhibit the anisotropic dispersion $\propto |\mathbf{q}|(\mathbf{B} \cdot \mathbf{q})$ at small wave vectors \mathbf{q} . If helicon-phonon interactions are neglected, the helicon dispersion intersects along a line with the phonon dispersion. Such an intersection always exists for acoustic phonons [see Fig. 1(c)], which are linearly dispersive for small \mathbf{q} . It also exists for optical phonons, which are gapped, if the magnetic field (cyclotron frequency ω_c) is sufficiently large [see Fig. 1(d)].

Unless wave vector \mathbf{q} is aligned with the direction of the magnetic field \mathbf{B} , helicons involve both transverse and longitudinal oscillations of electric current and electromagnetic fields. As a result, they interact with both longitudinal and transverse phonon modes and the mixed helicon-phonon excitations are separated by a gap [as shown in Figs. 1(b) and 1(f)]. In contrast, helicons propagating along the magnetic field \mathbf{B} are purely transverse circularly polarized waves (these corkscrew-shaped oscillations motivated the term “helicon”) and their coupling with the longitudinal phonon mode vanishes [cf. Figs. 1(a) and 1(e)]. As a result, dispersion relations for the mixed helicon-phonon excitations intersect at two selected points in reciprocal space and are of the Weyl nature in their vicinity.

The intersections of the dispersion relations for the mixed modes involving acoustic phonons and helicons have been known previously [18]. In this Letter, we demonstrate that

*dmitry.efimkin@monash.edu

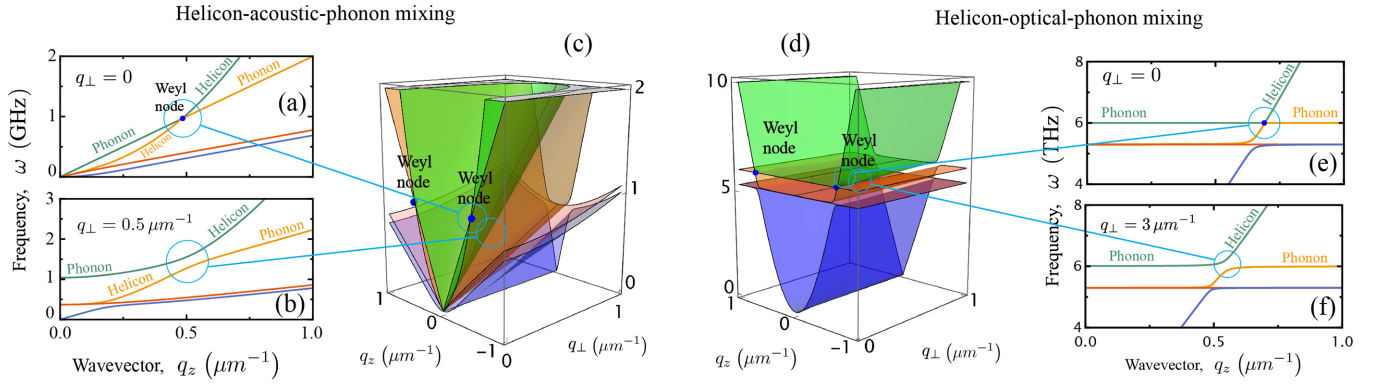


FIG. 1. The dispersion of hybrid modes emerging due to the hybridization of plasma waves with acoustic [(a)–(c)] and optical [(d)–(f)] phonons in a conductor in a magnetic field. The 3D plots (c) and (d) show the dispersion for as a function of the wave vectors q_z and q_\perp along and perpendicular to the magnetic field. The side panels are 2D plots of the dispersion as a function of q_z for different values of q_\perp . As a result of the hybridization of helicon and longitudinal-phonon branches, Weyl points emerge at $q_\perp = 0$, as shown in panels (a) and (c) for the case of acoustic phonons and in panels (d) and (e) for the case of optical phonons. The numbers on the axes are given for a potassium crystal in the magnetic field $B = 20$ T [(a)–(c)] and for heavily doped [39] CdSe with the electron density $n = 4 \times 10^{19} \text{ cm}^{-3}$ in the magnetic field $B = 45$ T [(d)–(f)].

they are of the Weyl nature and that such excitations also emerge for optical phonons. Furthermore, we show that Weyl excitations created by optical-phonon-Weyl hybridization can be readily observed in experiments and favor the emergence of arc surface modes.

Helicon waves. In the absence of phonons, the propagation of the Helicon waves is described by the linearized hydrodynamics equation

$$\partial_t \mathbf{j}(\mathbf{r}, t) = \frac{ne^2}{m} \mathbf{E}(\mathbf{r}, t) - \frac{e}{mc} [\mathbf{j}(\mathbf{r}, t) \times \mathbf{B}], \quad (1a)$$

complemented by the Maxwell equations

$$\text{curl } \mathbf{H}(\mathbf{r}, t) = \frac{4\pi \mathbf{j}(\mathbf{r}, t)}{c} + \frac{1}{c} \partial_t \mathbf{D}(\mathbf{r}, t), \quad (1b)$$

$$\text{curl } \mathbf{E}(\mathbf{r}, t) = -\frac{1}{c} \partial_t \mathbf{H}(\mathbf{r}, t), \quad (1c)$$

where e is the absolute value of the electron charge, n is the electron density, m is the effective mass, and c is the speed of light in vacuum. The magnetic field includes both the large external magnetic field $\mathbf{B} = B\mathbf{e}_z$ and a small oscillating component $\mathbf{H}(\mathbf{r}, t)$ created by propagating current density oscillations. For simplicity, we assume that the medium is nonmagnetic, i.e., has the magnetic permeability $\mu = 1$.

The helicon dispersion can be obtained from Eqs. (1a) and (1b) as a solution of the eigenvalue problem $\omega \psi_{\text{pl}} = \hat{\mathcal{H}}_{\text{pl}}(\mathbf{q}) \psi_{\text{pl}}$ [23–26] with the nine-component vector $\psi_{\text{pl}} = \{\sqrt{\epsilon_\infty} \mathbf{E}(\mathbf{q}), \mathbf{H}(\mathbf{q}), 4\pi \mathbf{j}(\mathbf{q})/\omega_p \sqrt{\epsilon_\infty}\}^T$, where $\omega_p = \sqrt{4\pi n e^2/m\epsilon_\infty}$ is the plasma frequency and ϵ_∞ is the contribution of the electronic shells of the atoms to the dielectric constants [at GHz and higher frequencies, $\mathbf{D}(\mathbf{r}, t) = \epsilon_\infty \mathbf{E}(\mathbf{r}, t)$]. The matrix $\hat{\mathcal{H}}_{\text{pl}}$ is given by

$$\hat{\mathcal{H}}_{\text{pl}}(\mathbf{q}) = \begin{pmatrix} 0 & -\bar{c} \hat{\mathcal{K}}_{\mathbf{q}} & -i\omega_p \hat{1} \\ \bar{c} \hat{\mathcal{K}}_{\mathbf{q}} & 0 & 0 \\ i\omega_p \hat{1} & 0 & -i\omega_c \hat{\mathcal{L}} \end{pmatrix}, \quad (2a)$$

where we have introduced the speed $\bar{c} = c/\sqrt{\epsilon_\infty}$ of electromagnetic waves in the material and the antisymmetric matrices $\hat{\mathcal{K}}_{\mathbf{q}}$ and $\hat{\mathcal{L}}$ are given by

$$\hat{\mathcal{K}}_{\mathbf{q}} = \begin{pmatrix} 0 & -q_z & q_y \\ q_z & 0 & -q_x \\ -q_y & q_x & 0 \end{pmatrix}, \quad \hat{\mathcal{L}} = \begin{pmatrix} 0 & 1 & 0 \\ -1 & 0 & 0 \\ 0 & 0 & 0 \end{pmatrix}, \quad (2b)$$

where $\omega_c = eB/mc$ is the cyclotron frequency.

The dispersion of the magnetoplasma modes is given by the positive ($\omega > 0$) eigenvalues of the “Hamiltonian” (2a). They include three gapped dispersion branches (longitudinal Langmuir waves and transverse circularly polarized L and R waves) with the gap of the order of the plasma frequency ω_p and a gapless branch, helicons (sometimes referred to as whistlers [38], cf. Fig. 2), on which we focus in the rest of the paper.

For small ratios ω_c/ω_p of the cyclotron to plasma frequencies, corresponding to realistic materials, the high-frequency modes can be excluded (see Supplemental Material, SM [39])

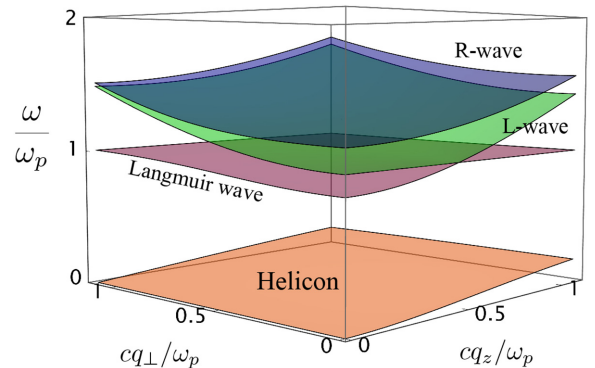


FIG. 2. The dispersion of plasma waves in an electron gas in a magnetic field for $\omega_c/\omega_p = 0.3$. They include three high-frequency modes (Langmuir, R, and L waves with frequencies around the plasma frequency ω_p) and the low-frequency helicon mode, whose dispersion is anisotropic and bounded by the cyclotron frequency ω_c .

for details) and the dynamics of helicons can be conveniently described using the three-component vector $\psi_{\text{hel}} = \{(B_x - iB_y)/\sqrt{2}, -B_z, (-B_x - iB_y)/\sqrt{2}\}$. The dispersion $\omega(\mathbf{q})$ of the low-energy excitations is given by the eigenvalue problem $\omega(\mathbf{q})\psi_{\text{hel}} = \hat{\mathcal{H}}_{\text{hel}}(\mathbf{q})\psi_{\text{hel}}$ with the matrix $\hat{\mathcal{H}}_{\text{hel}}(\mathbf{q})$ given by

$$\hat{\mathcal{H}}_{\text{hel}}(\mathbf{q}) = \alpha q_z \begin{pmatrix} q_z & \frac{q_x + iq_y}{\sqrt{2}} & 0 \\ \frac{q_x - iq_y}{\sqrt{2}} & 0 & \frac{q_x + iq_y}{\sqrt{2}} \\ 0 & \frac{q_x - iq_y}{\sqrt{2}} & -q_z \end{pmatrix}, \quad (3)$$

where $\alpha = \omega_c \bar{c}^2 / \omega_p^2 = Bc / 4\pi ne$.

By introducing the effective spin-1 operator $\hat{\mathbf{s}}$ in the space of vectors ψ_{H} , the operator (3) can be rewritten in the form $\hat{\mathcal{H}}_{\text{hel}}(\mathbf{q}) = \alpha q_z (\hat{\mathbf{s}} \cdot \mathbf{q})$ similar to the dispersion $\hat{H}_{\text{Weyl}} = v(\hat{\mathbf{s}} \cdot \mathbf{q})$ of a spin-1 Weyl semimetal [40]. The topological properties of the low-energy helicons are similar to those of spin-1 Weyl fermions. The operator (3) describes the helicon dispersion for small wave vectors $|\mathbf{q}| \ll \omega_p/c$. At larger wave vectors, the dispersion $\omega(\mathbf{q})$ with nonvanishing transverse wave vectors saturates to ω_c .

We note that helicons propagating (anti)parallel to the magnetic field \mathbf{B} have circular polarization in the plane perpendicular to \mathbf{B} . As we discuss below, the transverse polarization of helicons leads to the vanishing of the helicon-phonon interaction for both longitudinal acoustic and longitudinal optical phonons.

Interactions between helicons and acoustic phonons. In the absence of electrons, the dynamics of long-wave acoustic phonons is universally described in terms of the lattice displacement $\mathbf{u}(\mathbf{r}, t)$ by the equation of motion [41]

$$\partial_t^2 \mathbf{u}(\mathbf{r}, t) = s_l^2 \Delta \mathbf{u}(\mathbf{r}, t) + (s_l^2 - s_t^2) \nabla[\nabla \cdot \mathbf{u}(\mathbf{r}, t)] \quad (4a)$$

or the equivalent Hamilton's equations

$$\partial_t \mathbf{u}(\mathbf{q}, t) = \mathbf{p}(\mathbf{q}, t), \quad \partial_t \mathbf{p}(\mathbf{q}, t) = -(\hat{W}_{\mathbf{q}}^{\text{ac}})^2 \mathbf{u}(\mathbf{q}, t), \quad (4b)$$

where $\hat{W}_{\mathbf{q}}^{\text{ac}}$, $\mathbf{u}(\mathbf{q}, t)$ and $\mathbf{p}(\mathbf{q}, t)$ are the Fourier transforms of, respectively, $\hat{W}_{\mathbf{r}-\mathbf{r}'}$, $\mathbf{u}(\mathbf{r}, t)$ and $\mathbf{p}(\mathbf{r}, t)$. The momentum \mathbf{p} is the momentum canonically conjugate to the displacement \mathbf{u} ; s_l and s_t are the velocities of, respectively, longitudinal and transverse phonons; the matrix $\hat{W}_{\mathbf{q}}^{\text{ac}}$ (dynamical matrix) describes the energy

$$E_{\text{def}} = \frac{\rho}{2} \int d\mathbf{r} d\mathbf{r}' \mathbf{u}(\mathbf{r}, t) (\hat{W}_{\mathbf{r}-\mathbf{r}'}^{\text{ac}})^2 \mathbf{u}(\mathbf{r}', t) \quad (5)$$

of elastic deformations of the crystal where ρ is its mass density (see SM [39] for an explicit derivation of the dynamical matrix). The equations (4a) and (4b) can also be written as the eigenvalue problem $\omega\psi_{\text{ac}} = \hat{\mathcal{H}}_{\text{ac}}(\mathbf{q})\psi_{\text{ac}}$ with the six-component vector $\psi_{\text{ac}} = \{\mathbf{p}, \hat{W}_{\mathbf{q}}^{\text{ac}} \mathbf{u}\}$ and the matrix $\hat{\mathcal{H}}_{\text{ac}}(\mathbf{q})$ given by

$$\hat{\mathcal{H}}_{\text{ac}}(\mathbf{q}) = \begin{pmatrix} 0 & -i\hat{W}_{\mathbf{q}}^{\text{ac}} \\ i\hat{W}_{\mathbf{q}}^{\text{ac}} & 0 \end{pmatrix}. \quad (6)$$

The interactions between helicons and acoustic phonons come from relativistic effects ("inductive coupling" [18]). On the one hand, the dynamics of the crystalline lattice lead to the modification

$$\mathbf{E}(\mathbf{r}, t) \rightarrow \mathbf{E}(\mathbf{r}, t) + \frac{1}{c} [\partial_t \mathbf{u}(\mathbf{r}, t) \times \mathbf{B}] \quad (7)$$

of the electric field \mathbf{E} in the reference frame of the displaced atoms, where, in the long-wave limit under consideration, the displacement $\mathbf{u}(\mathbf{r}, t)$ varies smoothly compared to atomic length scales. The currents $\mathbf{j}(\mathbf{r}, t)$ in the helicon waves also lead the forces

$$\mathbf{f}(\mathbf{r}, t) = \frac{1}{c} [\mathbf{j}(\mathbf{r}, t) \times \mathbf{B}] \quad (8)$$

(per unit volume) acting on the lattice of the crystal and thus contributing to the displacements $\mathbf{u}(\mathbf{r}, t)$. Equations (7) and (8) describe the interactions between the electromagnetic field and the deformations of the lattice and thus account for the interactions between helicons and phonons.

The dynamics of coupled helicons and phonons is conveniently described by the 15-component vector $\psi_{\text{pl-ac}} = \{\sqrt{\varepsilon_{\infty}} \mathbf{E}, \mathbf{H}, 4\pi \mathbf{j} / \omega_p \sqrt{\varepsilon_{\infty}}, \sqrt{4\pi} \rho \mathbf{p}, \sqrt{4\pi} \rho \hat{W}_{\mathbf{q}}^{\text{ac}} \mathbf{u}\}^T$, where the first three vectors describe helicons [cf. Eqs. (1a)–(1c)] and the last two vectors describe the phonon degrees of freedom. The collective dispersion of coupled helicons and phonons is given by the solution of the eigenvalue problem $\omega\psi_{\text{pl-ac}}(\mathbf{q}) = \hat{\mathcal{H}}_{\text{pl-ac}}(\mathbf{q})\psi_{\text{pl-ac}}(\mathbf{q})$ with the "Hamiltonian" $\hat{\mathcal{H}}_{\text{pl-ac}}$ given by

$$\hat{\mathcal{H}}_{\text{pl-ac}} = \begin{pmatrix} 0 & -\bar{c}\hat{K}_{\mathbf{q}} & -i\omega_p \hat{1} & 0 & 0 \\ \bar{c}\hat{K}_{\mathbf{q}} & 0 & 0 & 0 & 0 \\ i\omega_p \hat{1} & 0 & -i\omega_c \hat{L} & i\gamma_{\text{ac}} \hat{L} & 0 \\ 0 & 0 & i\gamma_{\text{ac}} \hat{L} & 0 & -i\hat{W}_{\mathbf{q}}^{\text{ac}} \\ 0 & 0 & 0 & i\hat{W}_{\mathbf{q}}^{\text{ac}} & 0 \end{pmatrix}, \quad (9)$$

where the frequency $\gamma_{\text{ac}} = \omega_c \sqrt{nm/\rho}$ describes the strength of the coupling between helicons and acoustic phonons.

The structure of the matrix (9) can be understood as follows. The top left 3×3 block (whose each element is a 3×3 matrix) matches the matrix (2a) that describes the helicon degrees of freedom in the absence of phonons. The bottom right 2×2 block describes the dynamics of phonons and has eigenvectors that correspond to the harmonic modes of the crystal. The other terms describe the helicon-phonon coupling and are obtained from Eqs. (7) and (8) taking into account that $\partial_t \mathbf{u}(\mathbf{q}, t) = \mathbf{p}(\mathbf{q}, t)$.

The dispersions of the hybridized helicon-phonon excitations, given by the eigenvalues of the matrix (9), are plotted in Figs. 1(a)–1(c) for a crystal of potassium in the magnetic field $B = 20$ T. The character of helicon-phonon hybridization is qualitatively different for different branches of the dispersion of acoustic phonons. Helicons do not interact with the anti-symmetric combination of two transverse phonon modes. The interaction between helicons and the symmetric combination of the transverse phonon modes leads to a gap in the dispersion of the resulting excitations at all wave vectors.

By contrast, the interaction of longitudinal phonons with helicons vanishes for $\mathbf{q} \parallel \mathbf{B}$ and is finite for other wave vectors. Their hybridization leads to the formation of two dispersion bands that intersect at the wave vectors $\mathbf{q}_{\text{Weyl}}^{\pm} = \pm \mathbf{e}_z s_l / \alpha$, at which the frequencies of phonons and helicons match ($s_l |\mathbf{q}| = |\alpha q_z \mathbf{q}|$) and which are parallel to the magnetic field \mathbf{B} . The interactions lead to the splitting between the bands at all other wave vectors. Therefore, the interaction between helicons and the longitudinal phonons leads to the formation of Weyl excitations near the wave vectors $\mathbf{q}_{\text{Weyl}}^{\pm}$.

Near the Weyl points, the Hamiltonian of the Weyl excitations as a function of the wave vector $\mathbf{k} = \mathbf{q} - \mathbf{q}_{\text{Weyl}}^{\pm}$ measured from the Weyl points is given by

$$\hat{\mathcal{H}}_{\text{w}}^{\pm}(\mathbf{k}) = \frac{s_{\perp}}{\alpha} + \frac{3}{2}s_{\perp}k_z \pm \begin{pmatrix} \frac{1}{2}s_{\perp}k_z & is_{\perp}^{\text{ac}}k_{-} \\ -is_{\perp}^{\text{ac}}k_{+} & -\frac{1}{2}s_{\perp}k_z \end{pmatrix}, \quad (10)$$

where $k_{\pm} = k_x \pm ik_y$ and the matrix acts in the space of the phonon and helicon bands that are being hybridized. The transverse velocity of the Weyl excitations $s_{\perp}^{\text{ac}} = \gamma_{\text{ac}}\bar{c}/2\omega_{\text{p}}$ is determined by the strength of the helicon-phonons interactions. The Weyl nodes near the wave vectors $\mathbf{q}_{\text{Weyl}}^{\pm}$ have topological Chern numbers [12] $C^{\pm} = \frac{1}{2\pi} \int_S \nabla_{\mathbf{k}} \times \langle \psi_{+}(\mathbf{k}) | i \nabla_{\mathbf{k}} | \psi_{+}(\mathbf{k}) \rangle d\mathbf{S} = \mp 1$, where $\psi_{+}(\mathbf{k})$ is the eigenvector of the Hamiltonian (10) that describes the quasiparticle state with the wave vector \mathbf{k} and S is an arbitrary closed surface in reciprocal space surrounding the Weyl node.

Interaction between helicons and optical phonons. In certain materials, such as polar crystals or ionic semimetals, the elementary cell consists of positively and negatively charged ions, and electric polarization may be caused by a relative displacement of the atoms within the cell. This leads to strong interactions of helicons with optical phonons, which, unlike the case of acoustic phonons, are nonrelativistic in nature. Such interactions lead to the emergence of additional pairs of Weyl excitations, distinct from those generated by the interactions of helicons with acoustic phonons.

In what follows, we consider a crystal with two ions in the elementary cell and introduce the relative displacement $\mathbf{w}(\mathbf{r}, t)$ between the ions. Our results can be generalized to the case of an arbitrary number of atoms in the elementary cell. Due to a change in the electric polarization, the displacement \mathbf{w} affects the electric induction

$$\mathbf{D}(\mathbf{r}, t) = \varepsilon_{\infty} \mathbf{E}(\mathbf{r}, t) + 4\pi \chi \mathbf{w}(\mathbf{r}, t) \quad (11)$$

in the crystal, where ε_{∞} is determined by the polarization of the electron shells of the atoms in an electric field, and the quantity χ describes the response of the polarization to \mathbf{w} [42]. In the absence of helicons, the long-wave dynamics of displacement $\mathbf{w}(\mathbf{r}, t)$ are governed by the equation of motion [43]

$$\partial_t^2 \mathbf{w}(\mathbf{q}, t) = -(\hat{W}_{\mathbf{q}}^{\text{op}})^2 \mathbf{w}(\mathbf{q}, t) + \chi \mathbf{E}(\mathbf{q}, t), \quad (12)$$

where the dynamical matrix $\hat{W}_{\mathbf{q}}^{\text{op}}$ determines the dispersion of optical phonons (see SM [39] for a specific form of $\hat{W}_{\mathbf{q}}^{\text{op}}$) in the absence of phonon interaction with the electromagnetic fields.

Similarly to the case of acoustic phonons, the collective modes of helicons interacting with optical phonons can be obtained as a solution of the eigenvalues problem $\hat{\mathcal{H}}_{\text{pl-op}} \psi_{\text{pl-op}} = \omega \psi_{\text{pl-op}}$, where $\psi_{\text{pl-op}} = \{\sqrt{\varepsilon_{\infty}} \mathbf{E}, \mathbf{H}, 4\pi \mathbf{j}/\omega_{\text{p}} \sqrt{\varepsilon_{\infty}}, \sqrt{4\pi} \mathbf{p}, \sqrt{4\pi} \hat{W}_{\mathbf{q}}^{\text{op}} \mathbf{u}\}^T$. The resulting effective Hamiltonian $H_{\text{pl-op}}$ is given by

$$\hat{\mathcal{H}}_{\text{pl-op}} = \begin{pmatrix} 0 & -c\hat{K}_{\mathbf{q}} & -i\omega_{\text{p}}\hat{1} & -i\gamma_{\text{op}}\hat{1} & 0 \\ c\hat{K}_{\mathbf{q}} & 0 & 0 & 0 & 0 \\ i\omega_{\text{p}}\hat{1} & 0 & i\omega_{\text{c}}\hat{L} & 0 & 0 \\ i\gamma_{\text{op}}\hat{1} & 0 & 0 & 0 & -i\hat{W}_{\mathbf{q}}^{\text{op}} \\ 0 & 0 & 0 & i\hat{W}_{\mathbf{q}}^{\text{op}} & 0 \end{pmatrix}, \quad (13)$$

where $\gamma_{\text{op}} = \chi \sqrt{4\pi/\varepsilon_{\infty}}$ describes the strength of the coupling between helicons and optical phonons. The off-diagonal blocks in the matrix $\hat{\mathcal{H}}_{\text{pl-ac}}$ and $\hat{\mathcal{H}}_{\text{pl-op}}$, given by Eqs. (9) and (13), have different structure that reflects the distinct physical mechanisms of helicon interactions with acoustic and optical phonons.

In what follows, we neglect the dispersion of longitudinal and transverse optical phonons, i.e., assume that their frequencies ω_l and ω_t are momentum independent, which provides a good approximation for realistic crystals. Also, we assume that the frequencies ω_l and ω_t are of the same order of magnitude but differ. These assumptions are satisfied for semiconductors with the anisotropic wurtzite crystalline structure (e.g., CdSe, AlN, InN, etc.) [44] or in semiconductors with the zincblende structure (e.g., InAs, InSb, etc.) in the presence of a uniaxial strain. We also assume that the semiconductor crystal is heavily doped $\omega_1, \omega_c \ll \omega_{\text{p}}$ that implies dispersion curves for both helicons and optical phonons are well separated from the ones for high-frequency plasma Langmuir, R, and L waves [45].

The dispersion relations of excitations obtained as the eigenvalues of the matrix $\hat{\mathcal{H}}_{\text{pl-op}}$ are shown in Figs. 1(d)–1(f), with the numerical values of frequencies and wave vectors given for heavily doped CdSe for the magnetic field $B = 45$ T and electron concentration $n = 4 \times 10^{19} \text{ cm}^{-3}$ (see SM [39] for the details of the estimates).

Similarly to the case of acoustic phonons, the dispersions of noninteracting helicons and longitudinal optical phonons intersect along 2D lines, which for optical phonons are given by $\omega_l/\alpha = |q_z q|$. Interactions split these intersecting branches at all wave vectors other than $\mathbf{q}_{\text{Weyl}}^{\pm} = \pm \mathbf{e}_z \sqrt{\omega_l/\alpha}$ parallel to the magnetic field. Indeed, for this direction of wave vector, the electric field of helicon waves is orthogonal to the polarization and displacement of longitudinal phonons, and the helicon-phonon interaction vanishes. As a result, the hybridized helicon-phonon excitations have two bands that touch at the Weyl points at the wave vectors $\mathbf{q}_{\text{Weyl}}^{\pm}$. As a function of small deviations $\mathbf{k} = \mathbf{q} - \mathbf{q}_{\text{Weyl}}^{\pm}$ of momentum from Weyl points, the Hamiltonian of the Weyl excitations is given by

$$\hat{\mathcal{H}}_{\text{w}}^{\pm}(\mathbf{k}) = \omega_l + \sqrt{\alpha \omega_l} k_z \pm \begin{pmatrix} \sqrt{\alpha \omega_l} k_z & is_{\perp}^{\text{op}} k_{-} \\ -is_{\perp}^{\text{op}} k_{+} & -\sqrt{\alpha \omega_l} k_z \end{pmatrix}, \quad (14)$$

where $s_{\perp}^{\text{op}} = \gamma_{\text{op}} \omega_c c / 2\omega_{\text{p}}^2$ is the transverse velocity of Weyl excitations. The Weyl nodes near wave vectors $\mathbf{q}_{\text{Weyl}}^{\pm}$ have topological Chern numbers $C^{\pm} = \mp 1$.

Discussion. A prominent manifestation of the Weyl spectrum topology is a possible presence of protected surface arc states [1,2,10,12]. The existence of such arcs on the surface of a crystal requires that the excitations have a global gap in the reciprocal-space plane perpendicular to the surface. Provided that the global gap is present, the presence of the arc states is dictated by the bulk-edge correspondence [2].

In the case of acoustic phonons, the derived above Weyl excitations do not have such a gap and, therefore, lack arc surface states. By contrast, the dispersion of the mixed modes involving optical phonons has the global gap for any reciprocal-space section between the Weyl nodes. As for

the other sections, the global gap naturally appears if the optical phonons are dispersive (that is not captured by the hydrodynamic scheme we employ in this Letter). We can get insights into the behavior of the arc states if we consider the evolution of the mixed modes spectra with the longitudinal optical phonons frequency ω_1 treated as a free parameter. If ω_1 exceeds ω_c , longitudinal phonons and helicons do not intersect, and the Weyl nodes do not emerge. If ω_1 crosses ω_c and further decreases, the pair of Weyl nodes emerges at the infinity ($q_z \rightarrow \pm\infty$) and then moves towards $q_z = 0$. Thus, the surface arc states connect the projections of Weyl nodes in different Brillouin zones to the surface. The exact shape of the arcs away from their ends is nonuniversal and depends on the details of the phonon and helicon dispersion in the entire Brillouin zone.

The characteristic wave vectors and frequencies of Weyl excitations are very different in the cases of acoustic and optical phonons. For acoustic phonons, their mixing with helicons has been reported in potassium [46–48], aluminium [49], indium [50], lead telluride [51], and cadmium arsenide [52], is prominent within the MHz~GHz range and can be tuned by an external magnetic field. In the case of optical phonons, the frequencies of the Weyl excitations are determined by the frequencies of optical phonons that typically lie in the THz range. Good material candidates would have (i) low frequencies of optical phonons and at least a moderate splitting between their longitudinal and transverse modes and (ii) high mobilities of charge carriers. Among semiconductors extensively studied in the context of optoelectronics and plasmonics [53], these conditions are well satisfied for CdSe and strained InSb.

The discussed phonon-helicon excitations is a rather favourable playground for Weyl physics and observing associated fundamental phenomena. The predicted Weyl excitations are highly tunable, with the dispersion curves that can be tuned by the external magnetic field, strain, electric currents, etc. The relatively small momenta of these excitations allow for them to be readily excited by electromagnetic pulses in the THz and GHz ranges. The discussed systems present time-reversal-symmetry-breaking Weyl semimetals [2] (effectively, Weyl semimetal with only two symmetric Weyl cones, as

opposed to the so-called inversion-symmetry-breaking Weyl semimetals, in which the Weyl nodes lie, in general, at different energies). Such Weyl semimetals are extremely rare in solid-state materials and have not been observed until recently [54,55].

The predicted Weyl excitations and the surface arc states can be probed by phononic techniques (Raman and inelastic x-ray scattering experiments), as well as various techniques designed for plasmon-polaritons, including angle-resolved reflection experiment [23,56]. The unidirectional nature of the topological-surface-arc excitations is promising for applications in the context of topological and nonreciprocal plasmonics [57].

Conclusions and outlook. We have shown that a generic conductor in a magnetic field hosts Weyl excitations, which emerge as a result of the hybridization of helicon waves and phonons. Such Weyl excitations exist generically due to the interactions of helicons with acoustic phonons. In polar crystals, additional Weyl excitations may emerge due to the interactions of helicons with optical phonons.

In this paper, we considered the emergence of Weyl excitations in topologically trivial materials. Our approach can be extended to doped topological insulators and Weyl semimetals, in which helicons are impacted by anomalous electronic responses as well as axion electrodynamic effects [58,59].

In this paper, we neglected the effects of dissipation on the considered excitations, assuming quasiparticle and phonon scattering rates to be sufficiently smaller than the characteristic frequencies, which corresponds to realistic experimental conditions [39]. In principle, dissipation effects may not only result in the broadening of Weyl nodes but lead to new intriguing phenomena. It has been predicted, for example, that in plasmonic and photonic crystals, non-Hermitian perturbations of the effective Hamiltonian can make Weyl nodes evolve into nodal discs [60] and nodal rings [61]. We leave the studies of such effects and the conditions necessary for realizing them for future studies.

Acknowledgment. We acknowledge support from the Australian Research Council Centre of Excellence in Future Low-Energy Electronics Technologies (CE170100039).

-
- [1] X. Wan, A. M. Turner, A. Vishwanath, and S. Y. Savrasov, Topological semimetal and Fermi-arc surface states in the electronic structure of pyrochlore irridates, *Phys. Rev. B* **83**, 205101 (2011).
- [2] N. P. Armitage, E. J. Mele, and A. Vishwanath, Weyl and Dirac semimetals in three-dimensional solids, *Rev. Mod. Phys.* **90**, 015001 (2018).
- [3] S.-Y. Xu, I. Belopolski, N. Alidoust, M. Neupane, G. Bian, C. Zhang, R. Sankar, G. Chang, Z. Yuan, C.-C. Lee *et al.*, Discovery of a Weyl fermion semimetal and topological Fermi arcs, *Science* **349**, 613 (2015).
- [4] B. Q. Lv, H. M. Weng, B. B. Fu, X. P. Wang, H. Miao, J. Ma, P. Richard, X. C. Huang, L. X. Zhao, G. F. Chen, Z. Fang, X. Dai, T. Qian, and H. Ding, Experimental discovery of Weyl semimetal TaAs, *Phys. Rev. X* **5**, 031013 (2015).
- [5] B. Q. Lv, N. Xu, H. M. Weng, J. Z. Ma, P. Richard, X. C. Huang, L. X. Zhao, G. F. Chen, C. E. Matt, F. Bisti *et al.*, Observation of Weyl nodes in TaAs, *Nat. Phys.* **11**, 724 (2015).
- [6] S.-Y. Xu, I. Belopolski, D. S. Sanchez, C. Zhang, G. Chang, C. Guo, G. Bian, Z. Yuan, H. Lu, T.-R. Chang *et al.*, Experimental discovery of a topological Weyl semimetal state in TaP, *Sci. Adv.* **1**, e1501092 (2015).
- [7] S.-Y. Xu, N. Alidoust, I. Belopolski, Z. Yuan, G. Bian, T.-R. Chang, H. Zheng, V. N. Strocov, D. S. Sanchez, G. Chang *et al.*, Discovery of a Weyl fermion state with Fermi arcs in niobium arsenide, *Nat. Phys.* **11**, 748 (2015).
- [8] L. X. Yang, Z. K. Liu, Y. Sun, H. Peng, H. F. Yang, T. Zhang, B. Zhou, Y. Zhang, Y. F. Guo, M. Rahn *et al.*, Weyl semimetal phase in the non-centrosymmetric compound TaAs, *Nat. Phys.* **11**, 728 (2015).

- [9] N. Xu, H. M. Weng, B. Q. Lv, C. E. Matt, J. Park, F. Bisti, V. N. Strocov, D. Gawryluk, E. Pomjakushina, K. Conder *et al.*, Observation of Weyl nodes and Fermi arcs in tantalum phosphide, *Nat. Commun.* **7**, 11006 (2016).
- [10] M. Z. Hasan, S.-Y. Xu, I. Belopolski, and S.-M. Huang, Discovery of Weyl Fermion semimetals and topological Fermi arc states, *Annu. Rev. Condens. Matter Phys.* **8**, 289 (2017).
- [11] A. A. Burkov, Chiral anomaly and transport in Weyl metals, *J. Phys.: Condens. Matter* **27**, 113201 (2015).
- [12] A. Burkov, Weyl metals, *Annu. Rev. Condens. Matter Phys.* **9**, 359 (2018).
- [13] D. T. Son and B. Z. Spivak, Chiral anomaly and classical negative magnetoresistance of Weyl metals, *Phys. Rev. B* **88**, 104412 (2013).
- [14] S. V. Syzranov and L. Radzihovsky, High-Dimensional disorder-driven phenomena in Weyl semimetals, semiconductors, and related systems, *Annu. Rev. Condens. Matter Phys.* **9**, 35 (2018).
- [15] P. J. W. Moll, N. L. Nair, T. Helm, A. C. Potter, I. Kimchi, A. Vishwanath, and J. G. Analytis, Transport evidence for Fermi-arc-mediated chirality transfer in the Dirac semimetal Cd_3As_2 , *Nature (London)* **535**, 266 (2016).
- [16] A. C. Potter, I. Kimchi, and A. Vishwanath, Quantum oscillations from surface Fermi arcs in Weyl and Dirac semimetals, *Nat. Commun.* **5**, 5161 (2014).
- [17] B. Skinner, Coulomb disorder in three-dimensional Dirac systems, *Phys. Rev. B* **90**, 060202(R) (2014).
- [18] E. Kaner and V. Skobov, Electromagnetic waves in metals in a magnetic field, *Adv. Phys.* **17**, 605 (1968).
- [19] D. P. Morgan, Helicon waves in solids, *Phys. Status Solidi (b)* **24**, 9 (1967).
- [20] B. Yang, Q. Guo, B. Tremain, L. E. Barr, W. Gao, H. Liu, B. Béri, Y. Xiang, D. Fan, A. P. Hibbins, and S. Zhang, Direct observation of topological surface-state arcs in photonic metamaterials, *Nat. Commun.* **8**, 97 (2017).
- [21] Q. Guo, B. Yang, L. Xia, W. Gao, H. Liu, J. Chen, Y. Xiang, and S. Zhang, Three dimensional photonic Dirac points in metamaterials, *Phys. Rev. Lett.* **119**, 213901 (2017).
- [22] M. Li, J. Song, and Y. Jiang, Topological characteristic of Weyl degeneracies in a reciprocal chiral metamaterials system, *New J. Phys.* **23**, 093036 (2021).
- [23] W. Gao, B. Yang, M. Lawrence, F. Fang, B. Béri, and S. Zhang, Photonic Weyl degeneracies in magnetized plasma, *Nat. Commun.* **7**, 12435 (2016).
- [24] J. B. Parker, J. B. Marston, S. M. Tobias, and Z. Zhu, Topological gaseous plasmon polariton in realistic plasma, *Phys. Rev. Lett.* **124**, 195001 (2020).
- [25] Y. Fu and H. Qin, Topological phases and bulk-edge correspondence of magnetized cold plasmas, *Nat. Commun.* **12**, 3924 (2021).
- [26] J. B. Parker, Topological phase in plasma physics, *J. Plasma Phys.* **87**, 835870202 (2021).
- [27] A. Okamoto, S. Murakami, and K. Everschor-Sitte, Berry curvature for magnetoelastic waves, *Phys. Rev. B* **101**, 064424 (2020).
- [28] S. Park and B.-J. Yang, Topological magnetoelastic excitations in noncollinear antiferromagnets, *Phys. Rev. B* **99**, 174435 (2019).
- [29] P. Shen and S. K. Kim, Magnetic field control of topological magnon-polaron bands in two-dimensional ferromagnets, *Phys. Rev. B* **101**, 125111 (2020).
- [30] R. Takahashi and N. Nagaosa, Berry curvature in magnon-phonon hybrid systems, *Phys. Rev. Lett.* **117**, 217205 (2016).
- [31] X. Zhang, Y. Zhang, S. Okamoto, and D. Xiao, Thermal Hall effect induced by magnon-phonon interactions, *Phys. Rev. Lett.* **123**, 167202 (2019).
- [32] G. Go, S. K. Kim, and K.-J. Lee, Topological magnon-phonon hybrid excitations in two-dimensional ferromagnets with tunable Chern numbers, *Phys. Rev. Lett.* **123**, 237207 (2019).
- [33] S. Zhang, G. Go, K.-J. Lee, and S. K. Kim, SU(3) topology of magnon-phonon hybridization in 2D antiferromagnets, *Phys. Rev. Lett.* **124**, 147204 (2020).
- [34] R. R. Neumann, A. Mook, J. Henk, and I. Mertig, Thermal Hall effect of magnons in collinear antiferromagnetic insulators: Signatures of magnetic and topological phase transitions, *Phys. Rev. Lett.* **128**, 117201 (2022).
- [35] D. K. Efimkin and M. Kargarian, Topological spin-plasma waves, *Phys. Rev. B* **104**, 075413 (2021).
- [36] T. Karzig, C.-E. Bardyn, N. H. Lindner, and G. Refael, Topological polaritons, *Phys. Rev. X* **5**, 031001 (2015).
- [37] A. V. Nalitov, D. D. Solnyshkov, and G. Malpuech, Polariton \mathbb{Z} topological insulator, *Phys. Rev. Lett.* **114**, 116401 (2015).
- [38] D. G. Swanson, *Plasma Waves* (CRC Press, Boca Raton, FL, 2003).
- [39] See Supplemental Material at <http://link.aps.org/supplemental/10.1103/PhysRevB.108.L161411> for detailed derivations of the long-wavelength theories for helicons, phonons, and mixed helicon-phonon excitations; specific forms of the dynamical matrices $\hat{W}_{\mathbf{q}}^{\text{ac(op)}}$ for acoustic (optical) phonons; the list of material parameters used for calculations; and estimations of the quality factor for helicons in potassium and heavily doped CdSe. The Supplemental Material also contains the Refs. [62–64].
- [40] B. Bradlyn, J. Cano, Z. Wang, M. G. Vergniory, C. Felser, R. J. Cava, and B. A. Bernevig, Beyond Dirac and Weyl fermions: Unconventional quasiparticles in conventional crystals, *Science* **353**, aaf5037 (2016).
- [41] L. D. Landau and E. M. Lifshitz, *Theory of Elasticity*, Course of Theoretical Physics Vol. 7 (Pergamon Press, London, 1959).
- [42] For polar crystals, $\chi = \omega_l \sqrt{(\epsilon_0 - \epsilon_\infty)/4\pi}$ is usually parametrized in terms of the static dielectric constant ϵ_0 and its value ϵ_∞ in the high-frequency limit.
- [43] K. Huang, On the interaction between the radiation field and ionic crystals, *Proc. R. Soc. London A* **208**, 352 (1951).
- [44] We also assume that the external magnetic field is directed along the c axis of the crystal.
- [45] We note that the emergence of the Weyl helicon-phonon waves does not rely on this assumption. Instead, it ensures that the renormalization of phonon dispersion curves due to their interactions with the three gapped high-frequency magnetoplasma modes can be safely neglected and simplifies the analysis of the dispersion relations for the mixed excitations.
- [46] C. C. Grimes and S. J. Buchsbaum, Interaction between helicon waves and sound waves in potassium, *Phys. Rev. Lett.* **12**, 357 (1964).
- [47] A. Libchaber and C. C. Grimes, Resonant damping of helicon waves in potassium, *Phys. Rev.* **178**, 1145 (1969).

- [48] T. G. Blaney, The interaction between sound and helicon waves in potassium, *Philos. Mag.* **15**, 707 (1967).
- [49] P. Larsen and K. Saermark, Helicon excitation of acoustic waves in aluminium, *Phys. Lett. A* **24**, 374 (1967).
- [50] V. Gudkov, Rotation of polarization and ellipticity of ultrasound in helicon-phonon resonance conditions in indium, *Solid State Commun.* **44**, 229 (1982).
- [51] W. Schilz, Experimental evidence of bulk helicon-phonon coupling in PbTe, *Phys. Rev. Lett.* **20**, 104 (1968).
- [52] I. Rosenman, Helicon-phonon interaction in cadmium arsenide (Cd_3As_2), *Solid State Commun.* **3**, 405 (1965).
- [53] J. D. Caldwell, L. Lindsay, V. Giannini, I. Vurgaftman, T. L. Reinecke, S. A. Maier, and O. J. Glembocki, Low-loss, infrared and terahertz nanophotonics using surface phonon polaritons, *Nanophotonics* **4**, 44 (2015).
- [54] J.-Z. Ma, S. M. Nie, C. J. Yi, J. Jandke, T. Shang, M. Y. Yao, M. Naamneh, L. Q. Yan, Y. Sun, A. Chikina *et al.*, Spin fluctuation induced Weyl semimetal state in the paramagnetic phase of EuCd_2As_2 , *Sci. Adv.* **5**, eaaw4718 (2019).
- [55] N. Morali, R. Batabyal, P. K. Nag, E. Liu, Q. Xu, Y. Sun, B. Yan, C. Felser, N. Avraham, and H. Beidenkopf, Fermi-arc diversity on surface terminations of the magnetic Weyl semimetal $\text{Co}_3\text{Sn}_2\text{S}_2$, *Science* **365**, 1286 (2019).
- [56] D. Wang, B. Yang, W. Gao, H. Jia, Q. Yang, X. Chen, M. Wei, C. Liu, M. Navarro-Cía, J. Han *et al.*, Photonic Weyl points due to broken time-reversal symmetry in magnetized semiconductor, *Nat. Phys.* **15**, 1150 (2019).
- [57] K. Shastri, M. I. Abdelrahman, and F. Monticone, Non-reciprocal and topological plasmonics, *Photonics* **8**, 133 (2021).
- [58] F. M. D. Pellegrino, M. I. Katsnelson, and M. Polini, Helicons in Weyl semimetals, *Phys. Rev. B* **92**, 201407(R) (2015).
- [59] E. V. Gorbar, V. A. Miransky, I. A. Shovkovy, and P. O. Sukhachov, Pseudomagnetic helicons, *Phys. Rev. B* **95**, 115422 (2017).
- [60] W. Wang, W. Gao, L. Cao, Y. Xiang, and S. Zhang, Photonic topological fermi nodal disk in non-Hermitian magnetic plasma, *Light Sci. Appl.* **9**, 40 (2020).
- [61] A. Cerjan, S. Huang, M. Wang, K. P. Chen, Y. Chong, and M. C. Rechtsman, Experimental realization of a Weyl exceptional ring, *Nat. Photon.* **13**, 623 (2019).
- [62] C. Bungaro, K. Rapcewicz, and J. Bernholc, *Ab initio* phonon dispersions of wurtzite AlN, GaN, and InN, *Phys. Rev. B* **61**, 6720 (2000).
- [63] F. Widulle, S. Kramp, N. Pyka, A. Göbel, T. Ruf, A. Debernardi, R. Lauck, and M. Cardona, The phonon dispersion of wurtzite CdSe, *Phys. B: Condens. Matter* **263-264**, 448 (1999).
- [64] O. Madelung, in *Semiconductors Data Handbook* (Springer, Berlin, 2004), pp. 815–835.